Analysis of Electromagnetic Transmission through Dielectric filled Apertures of Arbitrary Shape in a Thick Conducting Screen

ABUNGU N ODERO[1], D B O KONDITI[1] AND A V OTIENO[2]

[1]Department of Electrical and Electronic Engineering
Jomo Kenyatta University of Agriculture and Technology
P.O. Box 62000, Nairobi
KENYA

[2] Department of Electrical and Electronic Engineering
University of Nairobi
KENYA

Abstract **–** The paper deals with an extension of the previous work appearing in a past issue of this transaction by the authors on hybrid FEM/MOM technique for analyzing transmission properties of arbitrarily shaped apertures on a thick conducting screen. In the present work, the effect of placing different dielectric material slabs in the conducting screen cavity on the electromagnetic transmission parameters is first analyzed and, then, the effect of interchanging the positions of these dielectric slabs relative to the incident field. Validation results for rectangular and cross-shaped slots are presented. Close agreement between our data and published data is observed. Further data has been generated for rectangular, circular, diamond-shaped and cross-shaped apertures.

Key-Words: **– Apertures of arbitrary shape, Dielectric-filled cavity, Different Dieletric slabs at arbitrary position, Hybrid FEM-MOM technique, Perfect conducting screen**

1 Introduction

THE FEM technique has been used by many workers to evaluate electromagnetic fields in closed regions [1] – [2] due to its ability to accurately model the physical features of an object to a scale much smaller than the wavelength of interest, particularly when dealing with the evaluation of near- field parameters such as , surface currents, input impedance and scattering parameters. The method also handles quite effectively complex inhomogeneities and is less computationally intensive than Finite-Difference Time-Domain (FDTDM) and Moment Method (MOM) because of its sparse and banded matrices. However, it requires an absorbing boundary for unbounded regions in order to satisfy radiation conditions at far-fields. On the other hand, MOM technique [3] – [5], is superior in handling unbounded problems due to its ability to satisfy Sommerfeld radiation conditions at infinity. The FDTM requires a fine subdivision of the computational domain for good resolution and is quite computationally intensive

However, recently, the greatest progress in computational electromagnetics has been in the development and application of hybrid techniques, such as FEM/MOM (finite element-moment method) and FDTM/MOM (finite-difference time-domain-moment method), Xingchao and Yuan [2] and Abungu, et al [6].

2 Problem Formulation

Fig.1. illustrates the geometry of the problem under consideration. The configuration consists of a cavity in a thick conducting screen having apertures at the top and bottom surfaces, denoted by Γ_1 and Γ_2, respectively.

The free space region above and below, z > 0 and z < -d planes are, hereafter, called regions A and B, respectively, and the volume occupied by the cavity (-d< z < 0) referred to as region C. Different layers of material slabs, each of the same thickness, are embedded in region C.

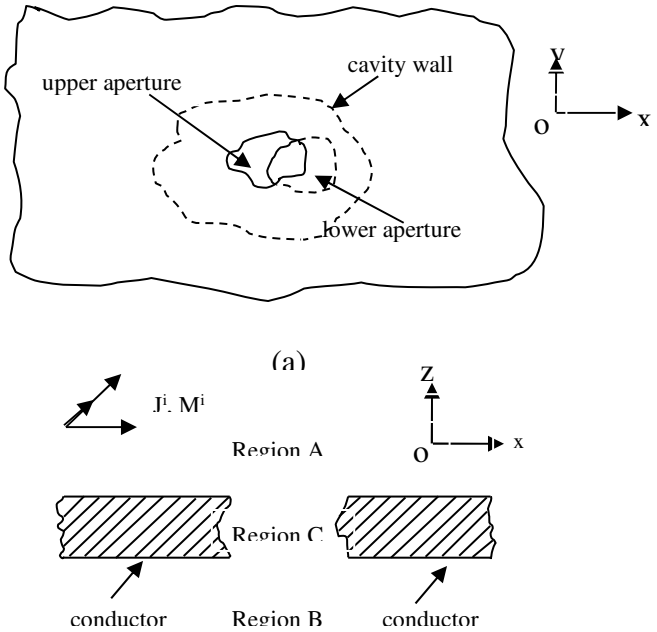

Fig.1 Problem geometry (a) Top view (b) Cross-sectional view

To decouple the fields in the three regions, the upper and lower apertures are closed with a perfect electric conductor (PEC) using an approach similar to that in [7], the tangential electric fields in the aperture planes, Γ_1 and Γ_2, are replaced with the equivalent magnetic currents $\overline{M}_1$ in the $z=0^+$ and $-\overline{M}_2$ in the $z=-d^-$ aperture planes, as illustrated in Fig.2. The problem geometry is then decomposed into 3 regions as illustrated in Fig.3. The magnetic field in regions A and B can be expressed as superposition of the short-circuited magnetic field $\overline{H}^{sc}$, which is the incident magnetic field plus the specular reflection from the PEC plane, and the scattered magnetic field $\vec{H}^{scat}$. On Γ_1 and Γ_2, the tangential components of the magnetic field can be expressed as

$$\hat{n}\times\overline{H}^{tot} = \hat{n}\times(\overline{H}^{sc}+\overline{H}^{scat}) \qquad (1)$$

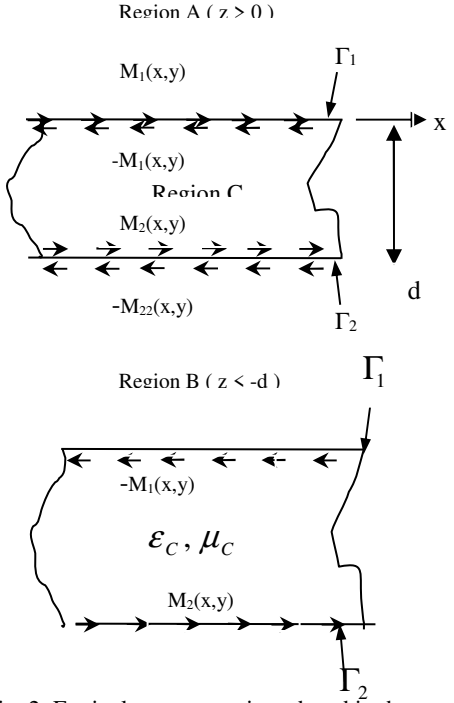

Fig. 2: Equivalent currents introduced in the aperture planes.

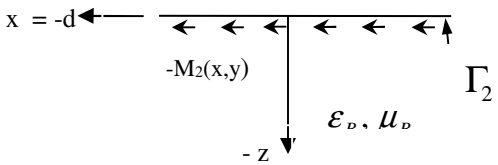

Fig. 3: Problem geometry decomposed into three regions; A, B, and C.

To maintain uniqueness in the solution, the tangential components of the magnetic field must be continuous across Γ_1 and Γ_2, within region C. Let

$$\overline{H}^{tot}(-\overline{M}_1)+\overline{H}^{tot}(\overline{M}_2)\ ;\ \overline{H}^{tot}(\overline{M}_2)+\overline{H}^{tot}(-\overline{M}_1) \qquad (2)$$

be the magnetic field on Γ_1 and Γ_2, respectively, produced by the equivalent

currents - $\overline{M}_1$ and $\overline{M}_2$.

By matching the tangential components of the exterior and interior magnetic fields on Γ_1 and Γ_2, Eq. (1) can be expressed as

$$\hat{n}\times\overline{H}^{sc} = \hat{n}\times(\overline{H}^{tot}(-\overline{M}_1)+\overline{H}^{tot}(\overline{M}_2)-\overline{H}^{scat}(\overline{M}_1)) \quad \text{on } \Gamma_1$$

$$\hat{n}\times\overline{H}^{sc} = \hat{n}\times(\overline{H}^{tot}(\overline{M}_2)+\overline{H}^{tot}(-\overline{M}_1)-\overline{H}^{scat}(\overline{M}_2)) \quad \text{on } \Gamma_2 \qquad (3)$$

for regions A and B, respectively. Eq. (3) is then solved using the method of moments following a similar procedure as in [5]. The equivalent currents are expanded into a series of known basis functions weighted by unknown coefficients. A set of vector testing functions, which are chosen to be the same as the basis functions (Galerkin procedure), is introduced.

2.1 Computing Exterior Admittance Matrices- MOM

The vector testing functions $\overline{W}_{m1}$ are distributed over Γ_1, and the functions $\overline{W}_{m2}$ over Γ_2.

Taking the inner product of Eq. (3) with the testing functions and taking the advantage of the linearity of the operators result in on Γ_1 given by Eq. (6)

similar expression can be derived for fields on Γ_2, with the equivalent magnetic currents $\overline{M}_1$ and $\overline{M}_2$ given as

$$\overline{M}_1(x,y,z=0)=\sum_{n=1}^{N}V_{1n}\overline{M}_{1n}(x,y) \qquad (7)$$

$$\overline{M}_2(x,y,z=-d)=\sum_{n=1}^{P}V_{2n}\overline{M}_{2n}(x,y) \qquad (8)$$

Now

$$[Y^A] = [<\vec{W}_{1m}, \vec{H}_{1t}^{scat}(\vec{M}_n)>]_{NxN} \qquad (9)$$

2.1.1 Matrix Elements Evaluation

As explained in [9], following Galerkin procedure ($\overline{W}_m = \overline{M}_m$), a typical matrix element for the r[th] region is given by

$$\begin{aligned} Y_{mn}^r &= 2<M_m, H_t^r(\overline{M}_n)> \\ &= 2\left\{\iint_{T_m^+}\overline{M}_m\bullet\overline{H}_t^r(\overline{M}_n)ds + \iint_{T_m^-}\overline{M}_m\bullet\overline{H}_t^r(\overline{M}_n)ds\right\} \\ &= 2\iint_{T_m^\pm}\overline{M}_m\bullet\overline{H}_t^r(\overline{M}_n)ds \end{aligned} \qquad (12)$$

where the notation $\iint_{T_m^+}(\quad)ds$ has been introduced for compactness.

In terms of the electric vector potential $\overline{F}(\bar{r})$ and the magnetic scalar potential $\phi(\bar{r})$, the magnetic field $\overline{H}^r(\overline{M}_n)$ can be written as (13)

$$<\overline{W}_{m1},\overline{H}_{1t}^{sc}>=-\sum_{n=1}^{N}V_{1n}<\overline{W}_{m1},(\overline{H}_{1t}^{tot}(-\overline{M}_{1_n})>+\sum_{n=1}^{p}V_{2n}<\overline{W}_{1m},\overline{H}_{1t}^{tot}(\overline{M}_2)>-\sum_{n=1}^{N}V_{1n}<\overline{W}_{m1},\overline{H}_{1t}^{scat}(\overline{M}_{1n})> \qquad (6)$$

Applying two-dimensional divergence theorem to

$$[Y^B] = [<\vec{W}_{2m}, \vec{H}_{2t}^{scat}(\vec{M}_p)>]_{PxP} \qquad (10)$$

$$\vec{I}^i = [-\langle\vec{W}_{1m}, \vec{H}_{1t}^{sc}\rangle]_{N\times 1} \qquad (11)$$

Eq. (12), leads to

$$\overline{H}^r(\overline{M}_n) = -j\omega\overline{F}_n(\bar{r})-\nabla\phi_n(\bar{r}) \qquad (13)$$

$$\overline{F}_n(\bar{r}) = \varepsilon^r\iint\overline{\overline{G}}(\bar{r}/\bar{r}')\bullet\overline{M}_n(\bar{r}')ds' \qquad (14)$$

$$\phi_n(\bar{r}) = \frac{\nabla\bullet\overline{F}_n(\bar{r})}{-j\omega\mu^r\varepsilon^r} \qquad (15)$$

$$Y_{mn}^r = -2j\omega\iint_{T_m^\pm}\overline{M}_m\bullet\overline{F}_n\,ds + 2\iint_{T_m^\pm}m_m\phi_n\,ds \qquad (16)$$

Eqn. (16) contains quadruple integrals; a double integral over the field triangles $T_m^\pm$ and a double integral over the source triangles $T_n^\pm$ involved in the computation of $\overline{F}_n(\bar{r})$ and $\phi_n(\bar{r})$. In order to reduce the numerical computations, the integrals over $T_m^\pm$ can be approximated by the values of integrals at the centroids of the triangles. This procedure yields

$$Y_{mn}^r = -2l_m\left\{\begin{array}{l} j\omega\left[\overline{F}_n(\bar{r}_m^{c+})\bullet\frac{\overline{\rho}_m^{c+}}{2}+\overline{F}_n(\bar{r}_m^{c-})\bullet\frac{\overline{\rho}_m^{c-}}{2}\right] \\ +\phi_n(\bar{r}_m^{c-})-\phi_n(\bar{r}_m^{c+}) \end{array}\right\} \qquad (17)$$

where $\overline{F}_n(\bar{r}_m^{c\pm}) = \varepsilon^r\iint_{T_n^\pm}\overline{\overline{G}}(\bar{r}^{c\pm}|\bar{r}')\bullet\overline{M}_n(\bar{r}')ds' \qquad (18)$

$$\phi_n(\bar{r}_m^{c\pm}) = \frac{-1}{j\omega\mu^r}\iint_{T_n^{\pm}}\left\{\nabla\bullet\overline{\overline{G}}(\bar{r}^{c\pm}\,|\,\bar{r}')\right\}\bullet\bar{M}_n(\bar{r}')ds' \qquad (19)$$

In (17), $\bar{\rho}_m^{c\pm}$ are the local position vectors to the centroids of $T_m^{\pm}$ and $\bar{r}_m^{c\pm} = (\bar{r}_m^{1\pm} + \bar{r}_m^{2\pm} + \bar{r}_m^{3\pm})/3$ are the position vectors of centroids of $T_m^{\pm}$ with respect to the global coordinate system.

Similarly, as explained in [9], using the centroid approximation in Eqn. (11), an element of excitation vector can be written as

$$I_m^i = -l_m\left\{\bar{H}_t^{\,i}(\bar{r}_m^{c+})\bullet\frac{\bar{\rho}_m^{c+}}{2} + \bar{H}_t^{\,i}(\bar{r}_m^{c-})\bullet\frac{\bar{\rho}_m^{c-}}{2}\right\} \qquad (20)$$

2.2 Computing Interior Admittance Matrix Y^C- FEM

Within the cavity region, the magnetic fields must satisfy the vector Helmholtz equation

$$\nabla\times\frac{1}{\varepsilon_r}\nabla\times\bar{H} - k^2\mu_r\bar{H} = 0 \qquad (21)$$

where $\bar{H}$ is the total magnetic field. The cavity region is defined as a closed space confined by PEC walls, which will be referred to as the domain V. A functional described by the inner product of the vector wave equation and the vectors testing function, $\bar{H}$, is expressed as

$$F(\bar{H}) = \iiint\left[\bar{H}^*\ast\nabla\times\frac{1}{\varepsilon_r}\nabla\times\bar{H} - k^2\mu_r\bar{H}^*\ast\bar{H}\right]dV \qquad (22)$$

is defined. The solution of the boundary-value problem is then found variationally, by solving for the magnetic field at a stationary point of the functional via the first variation

$$\delta F(\bar{H}) = 0 \qquad (23)$$

The functional has a stationary point (which occurs at an extremum) and equations (21) and (22) can be used to derive a unique solution for the magnetic field. For an arbitrary volume, V, the solution of the above variational expression cannot be found analytically and is derived via the FEM. To this end, the domain V is discretized into a finite number of subdomains, or element domains, V_e. Finite elements are chosen with lower degree that are compatible with the required regularity to minimize computational costs. Isoparametric tetrahedron elements (triangles on the surfaces and tetrahedrons for the volumes) with linear basis functions for the integral operators and for the differential surface and volume operators are chosen.

It is assumed that each element domain V_e has a finite volume and that the material profile within this volume is constant. Within each element domain the vector magnetic field is expressed as $\bar{H}_e$. If there are N_e element domains within V, the functional can be expressed in terms of the approximate magnetic fields as

$$F(\bar{H}) = \sum_{e=1}^{N_e}\left\{\iiint\left[\bar{H}_e^*\bullet\nabla\times\frac{1}{\varepsilon_r}\nabla\times\bar{H}_e - k_0^2\mu_r\bar{H}_e^*\bullet\bar{H}_e\right]dV_e\right\} \qquad (24)$$

$$\bar{H}_e^*\bullet\nabla\times\frac{1}{\varepsilon_r}\nabla\times\bar{H}_e = -\nabla.\left[\bar{H}_e^*\times\left(\frac{1}{\varepsilon_r}\nabla\times\bar{H}_e\right)\right] + \left(\frac{1}{\varepsilon_r}\nabla\times\bar{H}_e\right)\bullet\left(\nabla\times\bar{H}_e^*\right) \qquad (25)$$

Applying the vector identity

$$F(\bar{H}) = \sum_{e=1}^{N_e}\left\{\begin{array}{l}\iiint\left[\frac{1}{\varepsilon_r}(\nabla\times\bar{H}_e)^*\bullet.(\nabla\times\bar{H}_e) - k_0^2\mu_r\bar{H}_e^*\bullet\bar{H}_e\right]dV_e \\ +\iint\left[\frac{1}{\varepsilon_r}\bar{H}_e^*\bullet\hat{n}\times\nabla\times\bar{H}_e\right]dS_e\end{array}\right\} \qquad (26)$$

and the divergence theorem, (12) can be written as

$$\frac{1}{\varepsilon_{..}}\bar{H}_e^*.\hat{n}\times\nabla\times\bar{H}_e = j\frac{k_0}{\eta_0}\bar{H}_e^*\bullet\bar{M} \qquad (27)$$

implying contribution from only regions of implied magnetic current sources, i.e., at the apertures only. The approximate vector field in each element domain is represented as

$$\vec{H} = \sum_{j=1}^{m}\alpha_{ej}\vec{W}_{ej} \qquad (28)$$

with the spatial vector $\vec{W}_{ej}$ being the Whitney basis function defined by

$$\vec{W}_{ij} = \lambda_i\nabla\lambda_j - \lambda_j\nabla\lambda_i \qquad (29)$$

and λ_i is the barycentric function of node i expressed as

$$\lambda_i(\vec{r}) = \frac{1}{4} + \frac{(\vec{r}-\vec{r}_b).\vec{A}_i}{3V_e} \qquad (30)$$

where $\vec{A}_i$ is the inwardly directed vectorial area of the tetrahedron face opposite to node i, V_e the

element volume, and $\vec{r}$ the position vector. Also, $\vec{r}_b$ is the position vector of the barycenter of the tetrahedron defined as

$$\vec{r}_b = \frac{\left(\vec{r}_0 + \vec{r}_1 + \vec{r}_2 + \vec{r}_3\right)}{4} \tag{31}$$

in which $\vec{r}_i$ is the position vector of node i.

Using equations (29) in (28) leads to:

$$F\left(\vec{H}_e\right) = \sum_{e=1}^{N_e}\left\{\sum_{j=1}^{m}\alpha_{ej}^{*}\sum_{i=1}^{m}\alpha_{ei}\iiint\left[\frac{1}{\varepsilon_r}\left(\nabla\times\vec{W}_{ej}\right).\left(\nabla\times\vec{W}_{ei}\right)-k^2\vec{W}_{ej}.\vec{W}_{ei}\right]dV_e\right\}$$
$$-\sum_{b=1}^{N_b}\alpha_b^{*}\left\{j\frac{k_0}{\eta_0}\iint\vec{W}_b.\vec{M}_n dS\right\} \tag{32}$$

Letting

$$N_{ji} = \iiint\left[\frac{1}{\varepsilon_r}\left(\nabla\times\vec{W}_{ej}\right).\left(\nabla\times\vec{W}_{ei}\right)-k^2\vec{W}_{ej}.\vec{W}_{ei}\right]dV_e \tag{33}$$

and

$$P_{nb} = j\frac{k_0}{\eta_0}\iint\vec{W}_b.\vec{M}_n dS \tag{34}$$

equation (22) becomes

$$F\left(\vec{H}_e\right) = \sum_{e=1}^{N_e}\left\{\sum_{j=1}^{m}\alpha_{ej}^{*}\sum_{i=1}^{m}\alpha_{ei}N_{ji}\right\}-\sum_{b=1}^{N_b}\alpha_b^{*}P_{nb} \tag{35}$$

By enforcing the continuity of the magnetic field, a global number scheme can be introduced. The following symmetric and highly sparse matrix results

$$\begin{bmatrix}N_{ee} & N_{eb}\\ N_{be} & N_{bb}\end{bmatrix}\begin{bmatrix}\alpha_e\\ \alpha_b\end{bmatrix} = \begin{bmatrix}0\\ P_{nb}\end{bmatrix} \tag{36}$$

where: α_b are coefficients weighting the edge elements lying in the aperture plane Γ_1 and Γ_2. α_e are coefficients weighting the remaining edge elements in region C.

2.2.1 Computing Interior Matrix $\left[Y^C\right]$

The computation of the nth column of $\left[Y^C\right]$ in (6) and (7) is performed by perturbing the cavity with an equivalent current basis function M_n. Then, with the use of (21), the interior tangential magnetic fields in the aperture planes, Γ_1 and Γ_2, are computed. The first N row elements of the nth column of $\left[Y^C\right]$ are then computed by taking the inner product of the aperture field on Γ_1, successively with the N testing functions $\overline{W}_N$. The next P row elements of the nth column are computed by taking the inner product of the aperture field on Γ_2 with the P testing functions $\overline{W}_Q$. Similarly, the remaining P columns of $\left[Y^C\right]$ can be computed by perturbing the cavity with equivalent current basis functions M_p.

2.3 Complete Admittance Matrix

The complete admittance matrix from Eq. (13) can be expressed as

The advantage of using this function is that the admittance matrices of the interior and the exterior regions can be constructed independently.

$$\begin{bmatrix}\overline{H}_1^{sc}\\ \overline{H}_2^{sc}\end{bmatrix} = \begin{bmatrix}\left[Y_{11}^C\right] & \left[Y_{12}^C\right]\\ \left[Y_{21}^C\right] & \left[Y_{22}^C\right]\end{bmatrix}\begin{bmatrix}V_{1n}\\ V_{2n}\end{bmatrix} + \begin{bmatrix}\left[Y^A\right] & 0\\ 0 & \left[Y^B\right]\end{bmatrix}\begin{bmatrix}V_{1n}\\ V_{2n}\end{bmatrix} \tag{37}$$

The aperture admittance matrices $\left[Y^A\right]$ and $\left[Y^B\right]$ are computed by solving the problem of the equivalent magnetic currents radiating into a half-space. The aperture admittance matrix $\left[Y^C\right]$ is computed by solving the interior cavity problem.

Figs. 4 and 5 define the dimensions of cross-shaped and diamond-shaped aperture problems analyzed in this work.

3 Results and Conclusions

The formulation has first been validated by considering problems of rectangular, circular, diamond-shaped and cross-shaped apertures on thin conducting screens, as given in Table 1, based on the results of Konditi and Sinha [5] and for arbitrarily – shaped apertures on thick conducting screen of Abungu, et al [6] based on hybrid FEM-MOM, respectively. The results are seen to be in good agreement.

Thereafter, circular cross-shaped and diamond-shaped apertures in a screen of varying thickness and having two different dielectric layers filling the cavity have been studied. In each case equivalent magnetic current distributions and transmission cross-sections have been calculated. Relative permittivities for glass, titanium dioxide and air are taken as, 4.0, 96.0, and1.0, respectively.

The results obtained for different commutation of dielectric materials in the cavity region have been presented. Parameters computed are transmission cross-sections and equivalent magnetic currents.

It is observed in Figs. (6,7,8,9), that the thicker the cavity region the lower the transmission cross-section. Further, it has been established that the transmission cross-sections and magnetic current

magnitudes are larger if the incident wave approaches from the higher dielectric constant material toward the lower dielectric constant medium. This could be due to resonance occurring when an EM wave moves from higher dielectric constant material into a lower dielectric constant material. The phase of the equivalent magnetic current $\overline{M}$, on the other hand, is independent of the commutation of the dielectric slabs in the cavity region. This phenomenon seems to be consistent with Floquet's theorem, which states that given a plane wave incident on a periodic structure, all observable quantities will have the same periodicity as the structure and will have a cell-to-cell phase shift equivalent to that of the periodic structure.
.

References:

[1] C. M. Butler. Y. Rahmat-Samii. and R. Mittra,. Electromagnetic penetration through apertures in conducting surfaces, *IEEE Trans. Electromagn.* . vol. EMC-20. pp. 82-93, Feb. 1978.

[2] Xingchao Yuan, Three-dimensional electromagnetic scattering from inhomogeneous objects by the hybrid moment and the finite element method, *IEEE Trans Microwave Theory Tech.*, Vol. MTT-38, pp. 1053-1058, 1990.

[3] R.F. Harrington, J.R. Mautz, and D.T. Auckland: Electromagnetic coupling through apertures, Dept. Elec. Comput. Eng., Syracuse Univ., Syracuse NY, Rep. TR-81-4, Aug. 1981.

[4] David T. Auckland and Harington, R.F.: Electromagnetic transmission through a filled slit in a conducting plane of finite thickness, TE case, *IEEE Microwave Theory Tech.*, Vol.26, 499-505, July 1978

[5] Konditi, D.B.O. and Sinha, S. N.: Electromagnetic Transmission through Apertures of Arbitrary Shape in a Conducting Screen, *IETE Technical Review*, vol. 18, Nos. 2&3, March-June 2001, pp. 177-190.

[6] *Abungu, N. O.*, Konditi, D.B and Otieno, A.V.: Hybrid Method Analysis of Electromagnetic Transmission through Apertures of Arbitrary Shape in a Thick Conducting Screen, *WSEAS Trans. on Communications*, issue 6, vol.3, December 2004**,** pp.1767-1778

[7] Harrington, R.F. and Mautz, J.R.: A generalized network formulation for aperture problems, *IEEE Trans. Antennas Propagat.*, Vol. AP-24, pp. 870-873, 1976

[8] Harrington, R.F. Time–Harmonic Electromagnetic Fields. New York: McGraw-Hill, 1961.

[9] Rao, S.M., Wilton, D.R. and Glisson, A.W.: Electromagnetic scattering by surfaces of arbitrary shape, *IEEE Trans. Antennas Propagat.*, Vol. AP-30, pp.409-418, 1982

[10] D.B. Konditi, Moment method analysis of arbitrary-shape apertures in conducting screens and waveguides, Ph.D. Thesis, *IIT Roorkee*, 2000

Table 1: Validation Data

	Konditi & Sinha [3] - MOM Screen Thickness, t = 0.0λ		Abungu et al [5] Based on Hybrid FEM/MOM Screen thickness, t = 0.001λ	
1 Problem & Dimensions	Peak Equivalent Magnetic Current ($\overline{M}$)	Transmission Coefficient	Peak Equivalent Magnetic Current ($\overline{M}$)	Transmission Coefficient
Rectangular λ/20 x λ/2	13.4	0.33	13.2	0.32
Cross-shaped (A_w = 2L/3, L = h = 2λ/3)	3.3	1.3	3.1	1.2
Diamond-shaped L/λ = 0.8	22.0	0.77	-	-
Circular	1.25	1.65	1.15	1.55

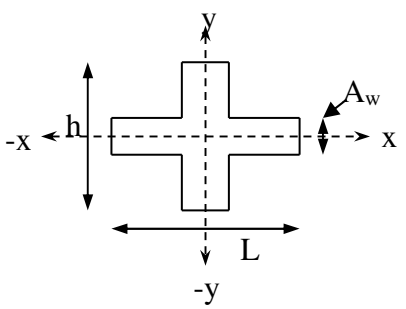

Fig. 4: Cross-shaped slot dimensions

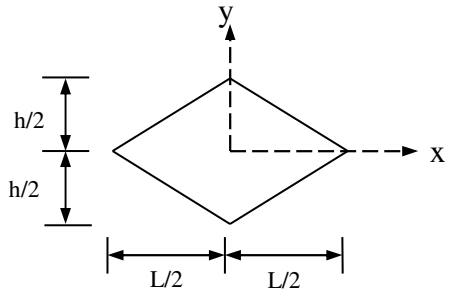

Fig.5: Diamond-shaped slot dimensions

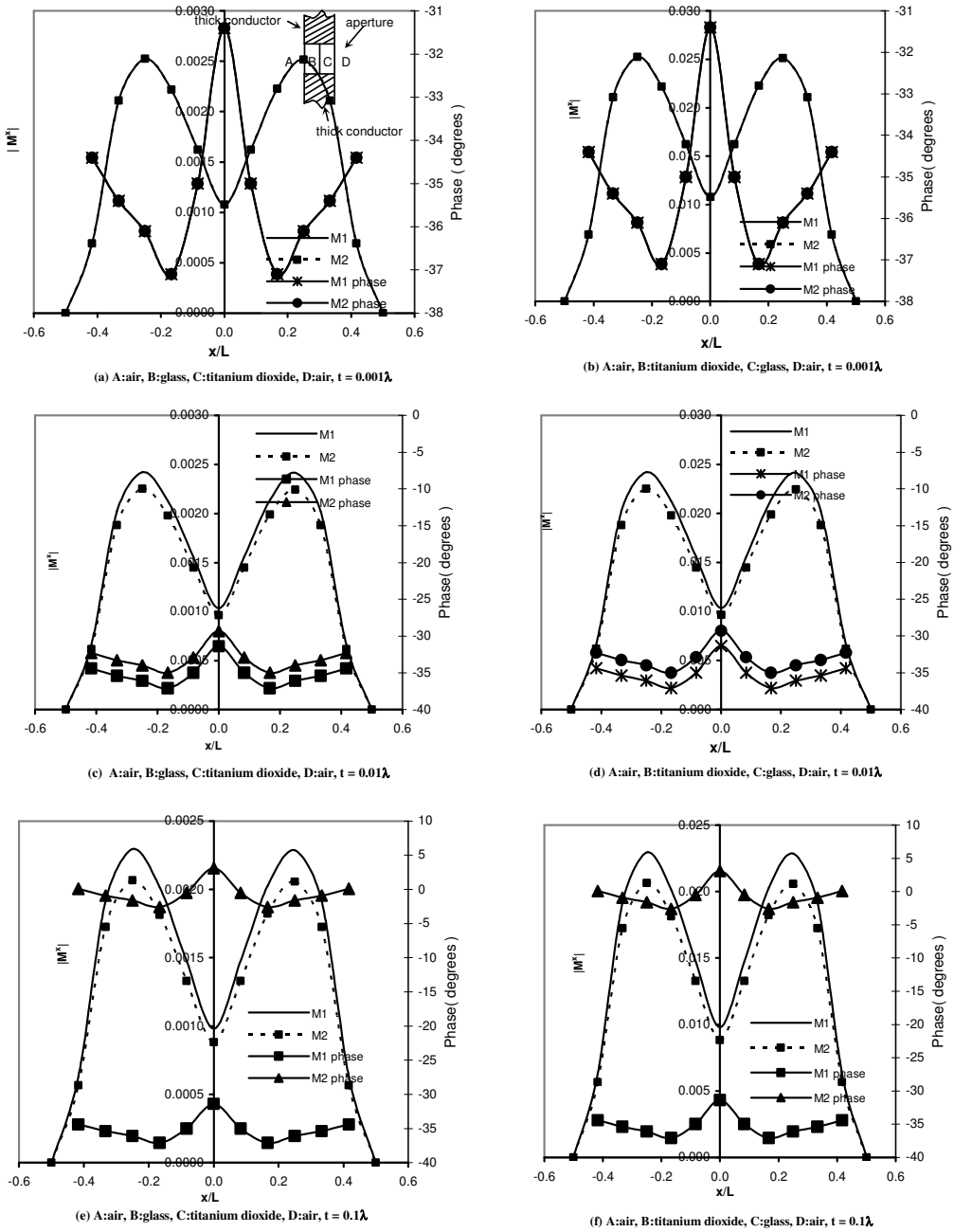

(a) A:air, B:glass, C:titanium dioxide, D:air, t = 0.001λ

(b) A:air, B:titanium dioxide, C:glass, D:air, t = 0.001λ

(c) A:air, B:glass, C:titanium dioxide, D:air, t = 0.01λ

(d) A:air, B:titanium dioxide, C:glass, D:air, t = 0.01λ

(e) A:air, B:glass, C:titanium dioxide, D:air, t = 0.1λ

(f) A:air, B:titanium dioxide, C:glass, D:air, t = 0.1λ

Fig.6: x-directed Surface Magnetic Current Distributions at y/h = -0.0625 for Aw = L/4 for Cross-shaped slots in a Conducting Screen of thickness t.

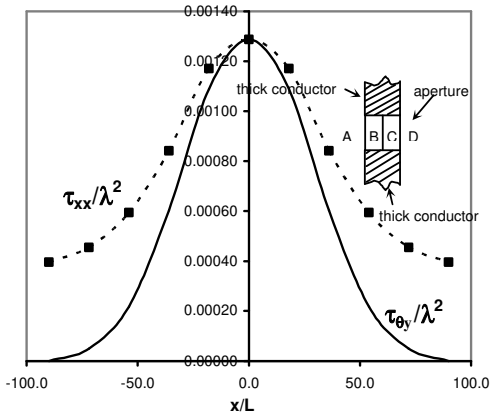

(a) A:air, B:glass, C:titanium dioxide, D:air, t = 0.001λ

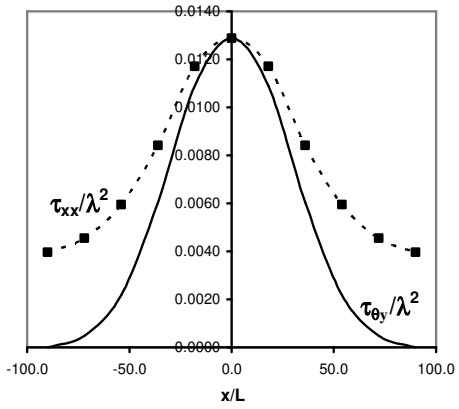

(b) A:air, B:titanium dioxide, C:glass, D:air, t = 0.001λ

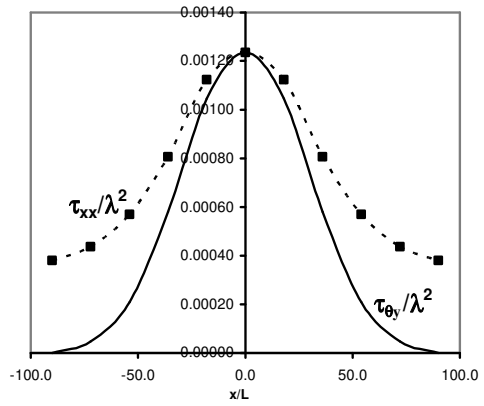

(c) A:air, B:glass, C:titanium dioxide, D:air, t = 0.01λ

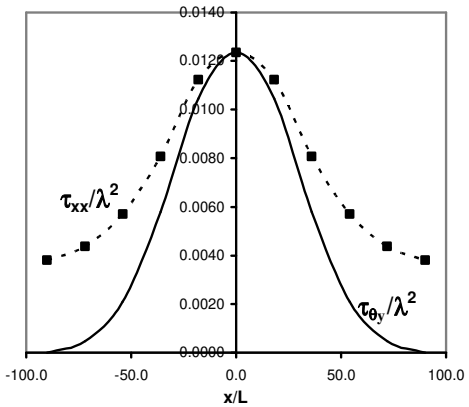

(d) A:air, B:titanium dioxide, C:glass, D:air, t = 0.01λ

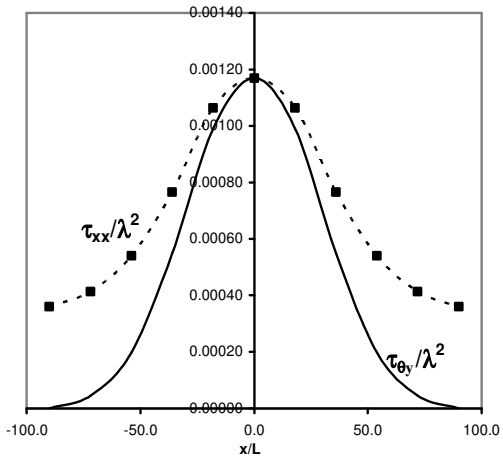

(e) A:air, B:glass, C:titanium dioxide, D:air, t = 0.1λ

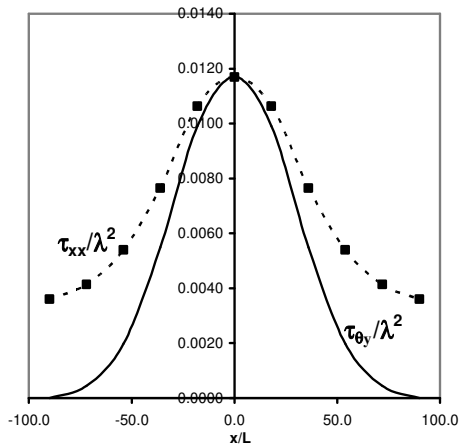

(f) A:air, B:titanium dioxide, C:glass, D:air, t = 0.1λ

Fig. 7: Transmission Cross-sections $\tau_{\theta y}/\lambda^2$ and τ_{xx}/λ^2 for inhomogeneously filled Cross-Shaped Slots, L = h = 2λ/3, Aw = L/4, in a Conducting Screen of thickness t.

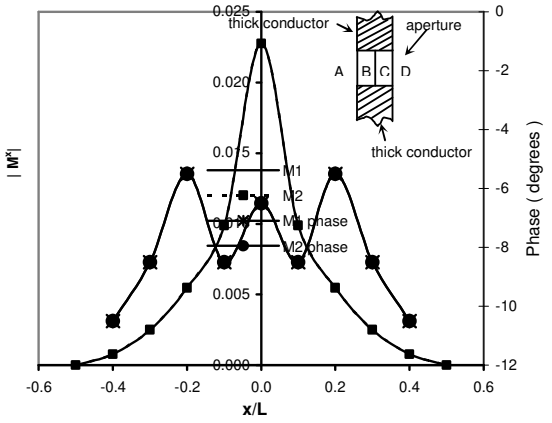

(a) A:air, B:glass, C:titanium dioxide, D:air, t = 0.001λ

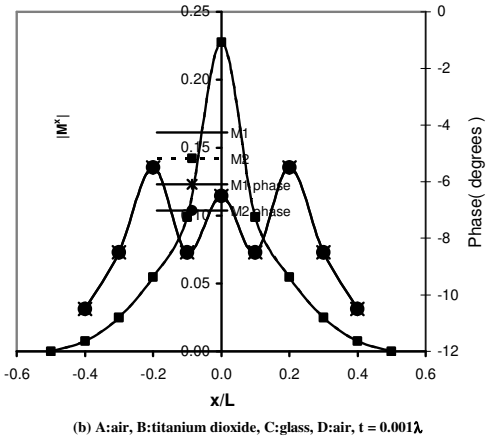

(b) A:air, B:titanium dioxide, C:glass, D:air, t = 0.001λ

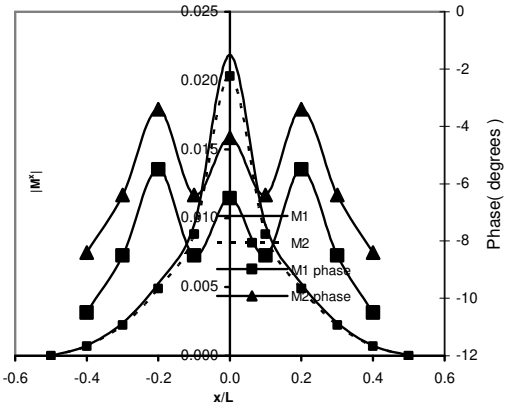

(c) A:air, B:glass, C:titanium dioxide, D:air, t = 0.01λ

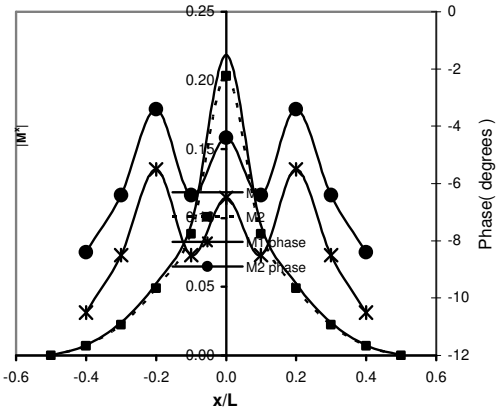

(d) A:air, B:titanium dioxide, C:glass, D:air, t = 0.01λ

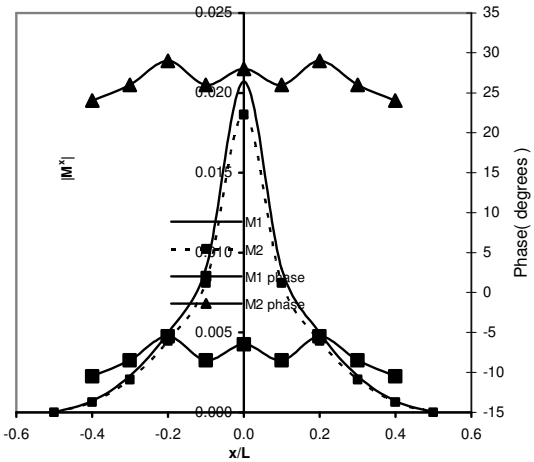

(e) A:air, B:glass, C:titanium dioxide, D:air, t = 0.1λ

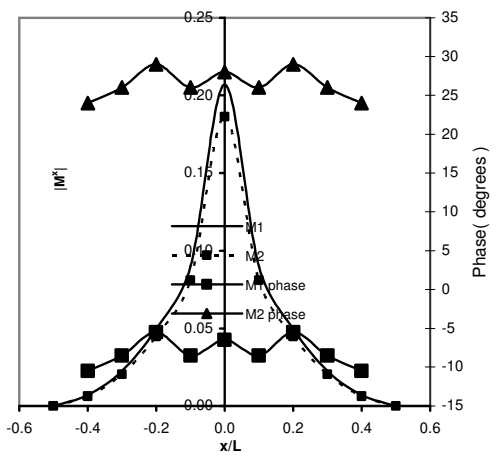

(f) A:air, B:titanium dioxide, C:glass, D:air, t = 0.1λ

Fig. 8: x-directed Surface Magnetic Current Distributions at y/h = -0.0833 for Diamond-shaped slots with h/λ = 0.3556 and L/λ = 0.8 in a Conducting Screen of thickness t.

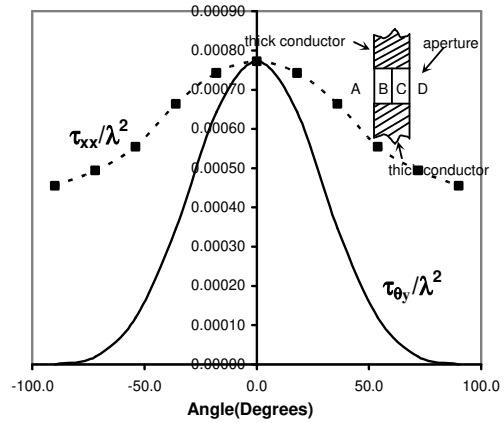

(a) A:air, B:glass, C:titanium dioxide, D:air, t = 0.001λ

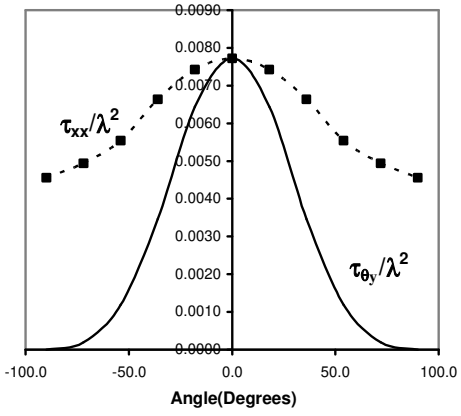

(b) A:air, B:titanium dioxide, C:glass, D:air, t = 0.001λ

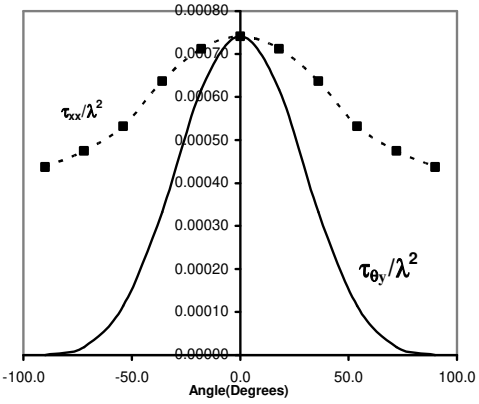

(c) A:air, B:glass, C:titanium dioxide, D:air, t = 0.01λ

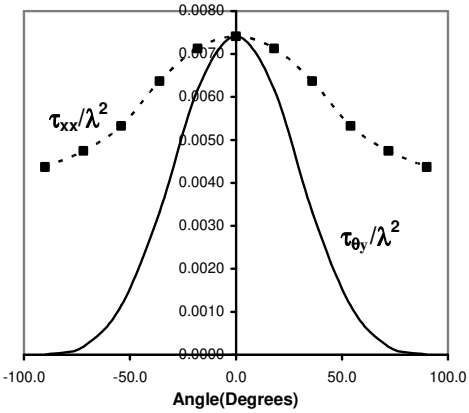

(d) A:air, B:titanium dioxide, C:glass, D:air, t = 0.01λ

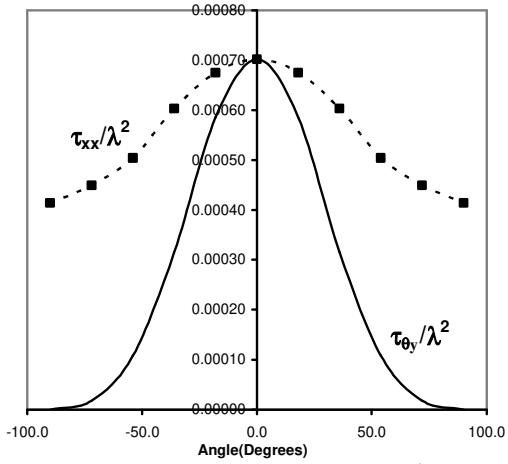

(e) A:air, B:glass, C:titanium dioxide, D:air, t = 0.1λ

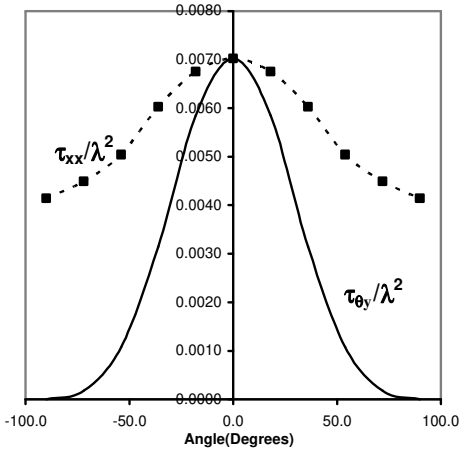

(f) A:air, B:titanium dioxide, C:glass, D:air, t = 0.1λ

Fig. 9: Transmission Cross-sections $\tau_{\theta y}/\lambda^2$ and τ_{xx}/λ^2 for inhomogeneously filled Diamond-Shaped Slots, $L/\lambda = 0.8$, in a Conducting Screen of thickness t.